Award number: 03HQGR0042

Paul Segall

Testing Earthquake Recurrence Models: Space-Time Patterns of Slip-Deficit at Parkfield

Program Element II - Research on Earthquake Physics and Effects.

Research supported by the U.S. Geological Survey (USGS), Department of the Interior, under USGS award number 03HQGR0042. The views and conclusions contained in this document are those of the authors and should not be interpreted as necessarily representing the official policies, either expressed or implied, of the U.S. Government.

03HQGR0042

TESTING EARTHQUAKE RECURRENCE MODELS: SPACE-TIME PATTERNS OF SLIP-DEFICIT AT PARKFIELD

Paul Segall
Geophysics Department
Stanford University
Stanford, CA 94305-2215
Phone: (650) 725-7241, **FAX:** (650) 725-7344
segall@stanford.edu, http://pangea.stanford.edu/research/CDFM/index.html

Key words: geodesy, Parkfield, transient deformation, silent earthquake

TECHNICAL ABSTRACT

In 1993 several baselines of the two-color EDM network at Parkfield, CA deviated from their long-term rates, coincident with anomalous observations from nearby strainmeters and a creepmeter, as well as an increase in microseismicity. Between October 1992 and December 1994 three M 4.5-5 earthquakes occurred beneath Middle Mountain, near the hypocenter of the 1934 and 1966 Parkfield M6 events. We analyzed the two-color EDM data using a Kalman-filtering based technique to image the spatio-temporal evolution of slip on the fault at Parkfield between the mid 1980s and 2003. This method accounts for localized random walk motion of the geodetic monuments and a prominent seasonal signal that affects many baselines. We find that a slip-rate increase occurred between January 1993 and July 1996 on the upper 8 km of the fault near Middle Mountain. The peak estimated slip rate during this time was 49 mm/yr, which exceeds the long-term geologic rate of ~35 mm/yr. The slip-rate evolution appears episodic, with an initial modest increase after the M4.3 earthquake and a much larger jump following the shallower M4.7 event in December, 1994. This temporal correlation between inferred slip and seismicity suggests that the moderate earthquakes triggered the aseismic fault slip. The EDM data cannot resolve whether transient slip propagated across the nucleation zone of the 1934 and 1966 M6 Parkfield earthquakes. However, transient slip and its associated stress release in the hypocentral area of previous Parkfield events is consistent with the nucleation of the 2004 M6 Parkfield earthquake elsewhere on the fault.

NONTECHNICAL ABSTRACT

Parkfield, a town located on the San Andreas fault in central California, is well-known for a series of M6 earthquakes that, until 1966, had occurred at approximately 22-year intervals. A prediction was made that another such earthquake would occur in 1988. However, the next M6 earthquake to follow the one in 1966 did not take place until 2004. One factor which may contribute to the temporal variability of earthquake recurrence at Parkfield and elsewhere is aseismic deformation, or movement on a fault that occurs slowly and therefore does not generate damaging seismic shaking.

In 1993 the data from several monitoring networks at Parkfield showed deviations from the long-term trends. One of these networks consisted of an electronic distance measuring (EDM) instrument used several times a week to record the distance between benchmarks located at different places near the San Andreas fault. These distances change if there is movement on the fault underground.

We analyzed data from the EDM network using a method that enables estimation of the temporal and spatial evolution of movement on the fault. The results show that the rate of movement, or slip, increased between January 1993 and July 1996 on the upper 8 km of the San Andreas, near the epicenter of the 1934 and 1966 Parkfield M6 earthquakes. The peak estimated slip rate during this time was 49 mm/yr, which exceeds the long-term rate of ~35 mm/yr.

The slip rate increase closely follows three moderate earthquakes that occurred on the same part of the fault between October 1992 and December 1994, suggesting that these earthquakes may have triggered the aseismic slip. Like a regular earthquake, aseismic slip releases stored stress on a fault, and therefore the aseismic slip at Parkfield may have influenced the ultimate initiation of the 2004 earthquake in a different location on the fault (~20 km to the southeast) from the previous two events.

INTRODUCTION

In fiscal year 2002 we received NEHRP funding for a two-part research project, and we obtained a continuation grant for fiscal year 2003. In the first of the two projects, which was completed in fiscal year 2002, we conducted a rigorous test of the time-predictable earthquake recurrence model at Parkfield, CA using geodetic data. Our findings show that the time-predictable model did not accurately forecast a subsequent M6 earthquake on the 1966 rupture plane. This simplified earthquake recurrence model does not account for many of the complexities that have been observed in several seismically-active areas. One of these is time-varying deformation. The second component of the project was to image the spatio-temporal evolution of slip on the San Andreas fault near Parkfield during the mid-1990s. We present the results of that work in this final report.

BACKGROUND

The unfulfilled prediction of a M6 Parkfield earthquake in 1988 ±5 years [*Bakun and Lindh,* 1985] focused attention on the seismo-tectonic processes that regulate the occurrence of moderate earthquakes there. In particular, it is important to determine whether there is evidence for a change in conditions during the 1966 - 2004 earthquake cycle that would produce the observed delay of the expected M6 event. In the early to mid-1990s creepmeter, strainmeter, and two-color electronic distance meter (EDM) observations deviated from their long-term trends [*Gwyther et al.*, 1996; *Langbein et al.*, 1999; *Nadeau and McEvilly*, 1999; *Gao et al.*, 2000; *Roeloffs*, 2001]. This was accompanied by an overall increase in moment release from microseismicity [*Nadeau and McEvilly*, 1999]. More recently, a concurrent magnetic anomaly has been identified in data from that time period [*Johnston and Mueller*, 2002]. Although the existence of such observations on a variety of instruments suggests a geophysical origin, the interpretation is complicated by the simultaneous occurrence of increased rainfall after several years of drought [*Roeloffs*, 2001].

Perhaps most intriguing is the coincidence of the deformation anomalies with the occurrence of three ~M4.5 – 5 earthquakes between 1992 and 1994, the biggest events at Parkfield since 1966. During the interseismic period, the hypocentral area of the 1966 and 1934 M6 earthquakes was largely aseismic and bracketed by two streaks of microseismicity [*Waldhauser et al.*, 2004]. The seismic events of the early 1990s initiated in the deeper of the two streaks and ruptured toward the 1966 hypocenter [*Fletcher and Spudich*, 1998; *Hellweg and Boatwright*, 1999]. Their temporal correlation with the geodetic anomalies suggests a relationship between the moderate earthquakes and aseismic fault slip.

A number of studies [*Gwyther et al.*, 1996; *Langbein et al.*, 1999; *Gao et al.*, 2000] have interpreted the strainmeter and two-color EDM data in terms of an increase in slip-rate on the San Andreas. A common feature of these is an inferred area of increased slip rate northwest of Carr Hill (Figure 1). The moment release of the transients inferred in these studies is equivalent to that of an M_w 4.3 – 5.5 earthquake. All of these studies relied on forward models or inversions of the data assuming constant deformation rates over fixed time intervals.

In this study we extend these geodetic analyses by estimating the space-time history of fault slip near Parkfield for the time period 1984 – 2003 from line-length measurements. We seek to determine whether the data require transient slip, and if so to estimate its time of onset, duration, location, and spatial extent. Such inferences, as they relate to patterns of microseismicity and moderate earthquakes, can provide insight into the interplay of seismic and aseismic fault slip.

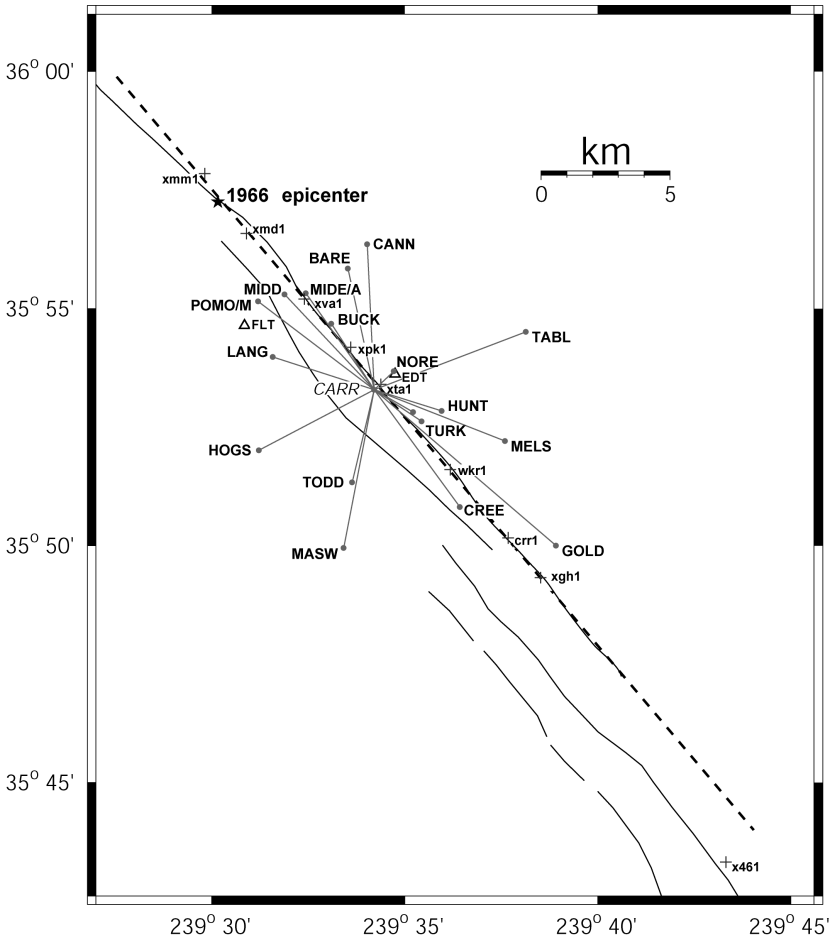

Figure 1 Parkfield permanent two-color EDM network. Central monument (CARR) is at Carr Hill. Solid black lines denote mapped fault trace. Dashed line marks the surface trace of the model fault plane used in the inversions. Epicenter of the 1966 M6 earthquake is shown for reference. Monument FLAT is unlabelled for figure clarity; The CARR-FLAT line is nearly parallel to the CARR-TURK line, but slightly shorter. MIDE/A and POMO/M each refer to a pair of baselines; POMM and MIDA have braced monuments which offer improved stability. These were installed close to POMO and MIDE in 1993 [*Langbein et al.,* 1995]. The locations of creepmeters are indicated by crosses. The two borehole tensor strainmeters, FLT and EDT, are shown by triangles.

DATA

The observations used in this study consist of line-length measurements from the permanent two-color EDM network at Parkfield [*Langbein et al.*, 1987; *Langbein, et al.*, 1990]. The core of this network is a laser geodimeter, located at Carr Hill (Figure 1), which modulates signals on both red and blue optical carrier frequencies. Measurements are made to a radial network of retroreflectors surrounding Carr Hill. The network was established in 1984, and measurements were made 2-3 times a week through the 1990s.

The detrended time series for fault-crossing baselines are shown in Figure 2. Several lines (e.g., BUCK, CANN, HUNT, GOLD, MELS, and TURK) show an apparent rate-change in April 1993. It is apparent from this figure that many lines experience strong seasonal variations which need to be accounted for in the analysis. The amplitudes of local seasonal displacements also display a range of behavior both in space and time, and some of the larger deviations are known to be correlated with heavy rainfall (e.g., line BARE in 1995 [*Langbein and Johnson*, 1997]). The displacements of the reflector monuments used for these observations are also known to exhibit random walk noise due to minor instabilities of the monuments in the surrounding soil. On average the standard deviation of the random walk is ~0.0013 m/(yr)$^{1/2}$, although some lines are much less stable [*Langbein and Johnson*, 1997; *Langbein*, 2004].

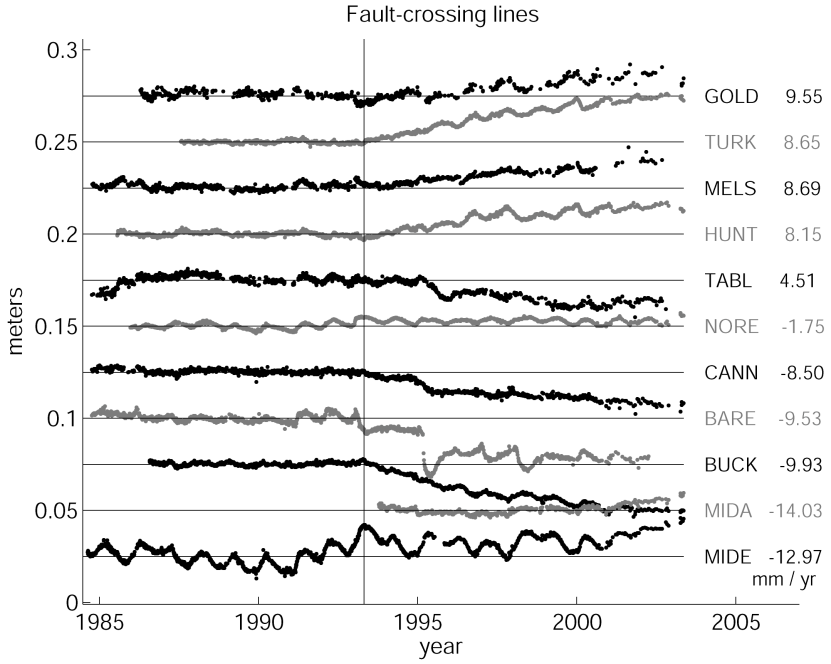

Figure 2 Time series for fault-crossing lines of the Parkfield permanent two-color EDM network detrended using data up to April 26, 1993 (vertical line). This date was chosen for purposes of display based on visual inspection of the time series. Black and gray are used to improve clarity. An obvious rate change occurs in April 1993 on several lines. The constant rate (in mm/yr) used to detrend each line is given to the right of the endpoint monument name. In August, 2000 the permanent two-color EDM instrument at Carr Hill was replaced by a portable instrument, and the observations became less frequent. The scatter in the data increases after this time. The average 1σ measurement errors are 0.5 mm prior to August, 2000 and 1.3 mm afterwards.

METHOD

Our analysis utilizes the Kalman filtering-based method termed the "Extended Network Inversion Filter" (ENIF) discussed by *McGuire and Segall* [2003] based on earlier work by *Segall and Matthews* [1997]. A key feature of *Segall and Matthews'* [1997] formulation is that it exploits the spatial coherence of a crustal deformation signal to separate it from time-varying noise which is local to each station. In the case of the EDM measurements used here, these noise sources include benchmark instability and annual variations most likely due to seasonal wetting and drying of the soil [*Langbein and Johnson*, 1997; *Langbein*, 2004].

A Kalman filter requires two models. The first embodies the time progression of the process of interest, and the second relates the time-varying process to the data. The model for time-progression is used to predict the data at epoch $k+1$ based on the model found using data up to epoch k. The data from epoch $k+1$ are used to improve upon the predicted model parameters through the observational model. This process is repeated for all observation epochs. Only the previous epoch's parameter estimates are used in predicting the current state. Furthermore, only the data from the current epoch are used to improve upon the prediction. Therefore new data are efficiently incorporated into the analysis, making Kalman filtering ideal for estimation of an ongoing process.

In the ENIF, the temporal variation of fault slip is modeled as an integrated random walk process. The local benchmark motion is treated as a random walk process, consistent with observed spectra of benchmark wobble [*Langbein*, 2004]. The annual seasonal noise is modeled as a sum of sine and cosine terms with time varying amplitudes. The temporal variation of the amplitudes is modeled as a random walk process.

The observed changes in line-length for the Parkfield two-color EDM network are modeled as the sum of contributions from fault slip, random walk benchmark motion, and seasonal signals. Different amounts of random walk and seasonal noise are estimated for each baseline. Fault slip is modeled as the sum of steady-state and transient displacement on a dislocation in a homogeneous, linear, elastic half-space. Slip is mapped linearly to displacement through the matrix of dislocation Green's functions, G (e.g., *Okada*, [1985]).

Following *Harris and Segall* [1987] and *Murray et al.* [2001], the San Andreas near Parkfield is approximated by a 39 km long vertical fault extending from the surface to 14 km depth. The model fault strikes N41^{o}W, and its location is shown by the dashed line in Figure 1. This fault geometry is based on geologic mapping [*Lienkaemper and Brown*, 1985; *Sims*, 1990], the spatial distribution of microseismicity [*Eaton et al.*, 1970; *Eberhart-Phillips and Michael*, 1993], and the inferred rupture area of the 1966 earthquake [*Segall and Du*, 1993]. In order to image spatial variations in fault slip, we discretize the model fault into a grid of uniformly sized blocks (3 km long by 2 km wide). The neighboring creeping and locked sections of the fault are represented by large dislocations (100 km long by 14 km wide) with uniform slip-rate. The contribution of motion on the portion of the fault below 14 km, which is assumed to represent deep slip and far-field plate motion, is accommodated by a uniformly-slipping dislocation 1000 km long and wide [*Savage*, 1990].

Spatial smoothing was applied to the estimated slip distribution at each epoch using a finite difference Laplacian operator. Purely strike-slip motion was assumed, and non-negativity constraints were imposed to ensure right lateral slip. Parameters that control the relative weighting of the data and the spatial smoothing and non-negativity constraints, as well as the temporal variability of the estimated slip and noise sources, are simultaneously estimated by the ENIF during filtering. Constraints from creepmeter observations were applied to the surface-breaking subfaults.

RESULTS

The results of the time-dependent inversion show a slip-rate increase northwest of Carr Hill at a depth of 2 - 8 kilometers between early 1993 and mid 1996. Figure 3 displays this solution at 16 epochs throughout the observation period. The imaged slip-rate history (sum of background steady-state rate and transient rate) reaches a maximum of 49 mm/yr in late 1994 to

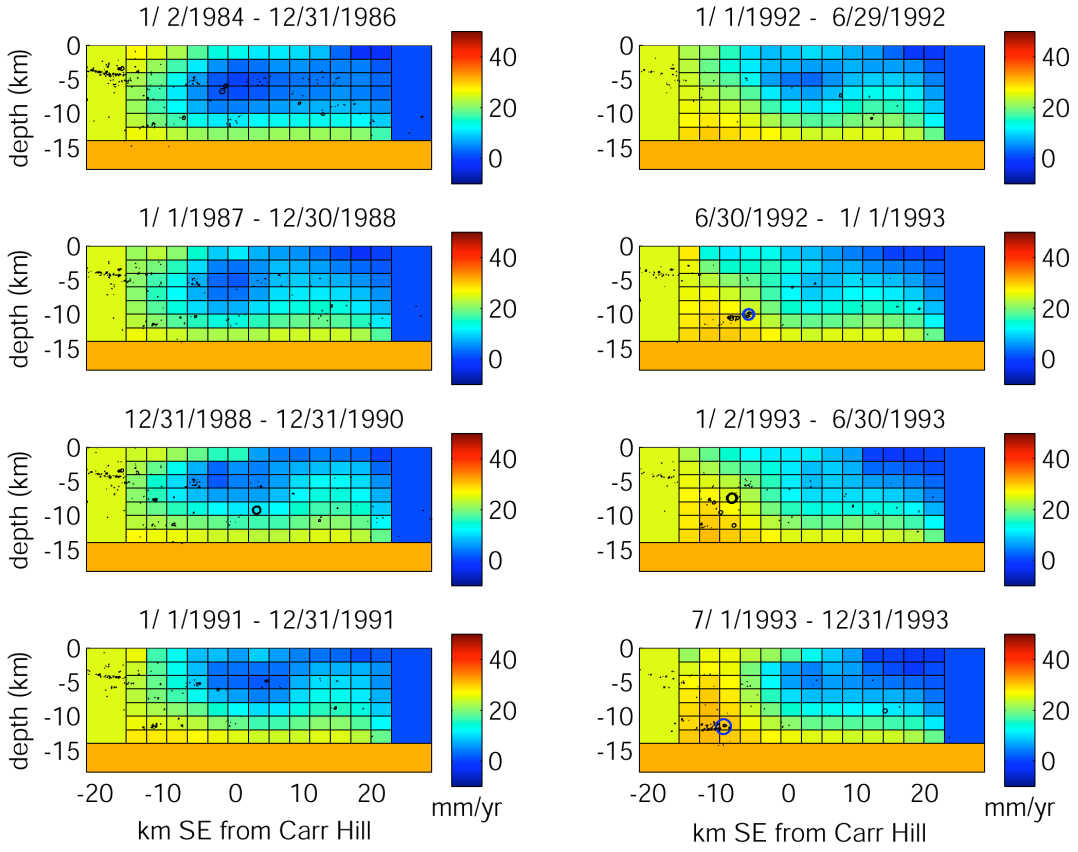

Figure 3a Time history of estimated slip-rate distribution. Each frame shows the distribution of slip-rate (secular plus transient) at the end of the indicated time interval. Carr Hill (the location of the two-color network's central monument, near the town of Parkfield) is located at zero on the horizontal axis. Superimposed on each frame are the precise relative relocations of microseismicity occurring during the indicated time-interval [*Waldhauser et al.*, 2004]. The microseismicity is plotted as the equivalent rupture area of a 3 MPa stress-drop crack. The M 4.3 Oct. 20, 1992, M 4.6 Nov. 14, 1993, and M 4.7 Dec. 20, 1994 earthquakes [*Fletcher and Spudich*, 1998] are shown in blue. Note area of increased slip-rate on the NW end of the fault plane commencing in early 1993.

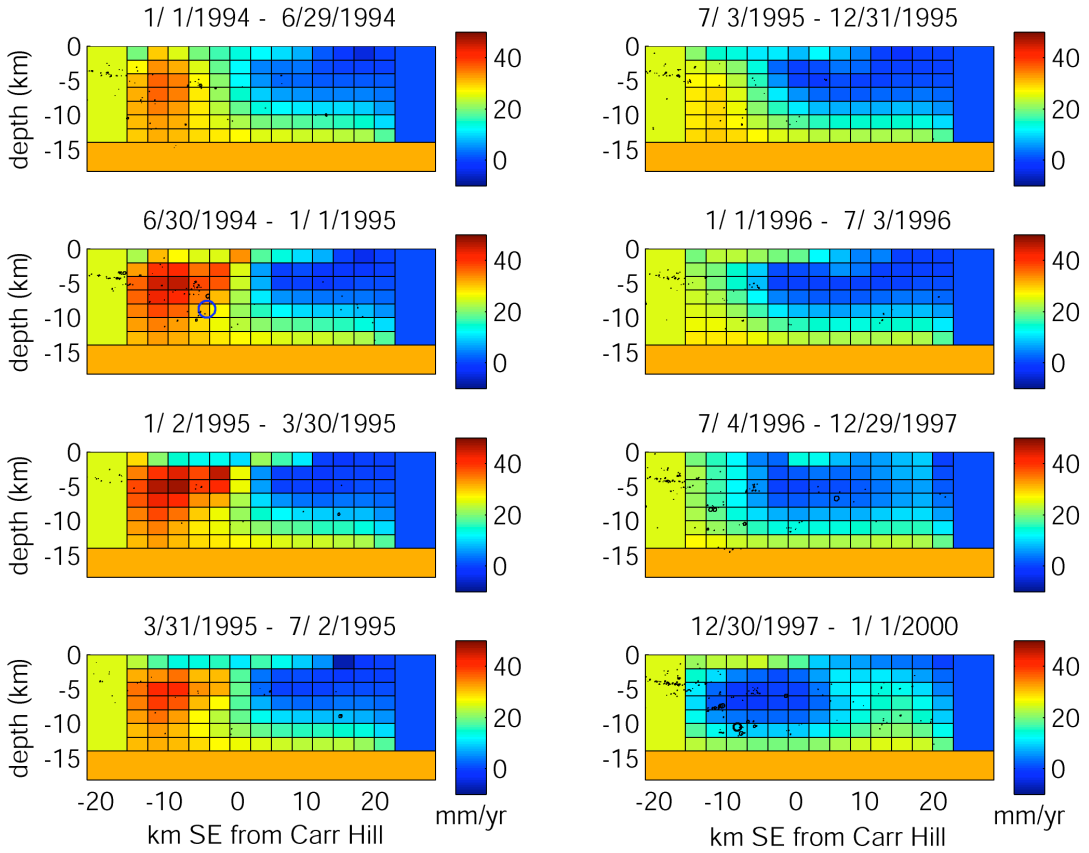

Figure 3b Time history of estimated slip-rate distribution, continued.

early 1995. As can be seen in Figure 3, the slip-rate increase appears to initiate at depths of ~12 km and then move upward, finally concentrating around 6 km depth (Figure 3b). However, given the limited power of the EDM data to resolve slip-rates on the deeper part of the fault plane, the conclusion that transient slip propagated upward is not robust.

The solution presented in Figure 3 is conditional on all the data (rather than only the observations available up to and including a given epoch) through back-smoothing [*Rauch et al.*, 1965]. Although smoothing reduces the model variance, it also obscures rapid changes in slip-rate and tends to shift the peak slip-rate estimates backward in time. Figure 4 shows the inferred moment-rate history for the portions of the fault northwest and southeast of Carr Hill found in the forward run of the filter (i.e., without smoothing).

Between 1992 and 1994 a series of M>4 earthquakes occurred in the vicinity of Middle Mountain. These events (Oct. 20, 1992, M4.3; Nov. 14, 1993, M4.6; and Dec. 20, 1994, M4.7) are shown by blue circles between -4 and -10 km along strike in Figure 3. The moment-rate exhibits a modest increase following the first of these earthquakes (in October, 1992) and a dramatic increase after the largest of these events (in December, 1994). Based on the forward filter slip-rate solution, we estimate that the increased slip rate northwest of Carr Hill began with

the October 1992 earthquake and lasted until July 1996. The moment released during this time span northwest of Carr Hill was found to be 2.7 x 10^{17} Nm, equivalent to that of a Mw 5.6 earthquake. Tests using simulated data for the Parkfield two-color EDM network verified that the ENIF is capable of detecting an event of this size. Based on published slip distributions [*Fletcher and Spudich*, 1998], the predicted surface displacement due to the largest of the three earthquakes does not exceed 1 mm, so the coseismic contribution to the observed EDM signal from these events is negligible.

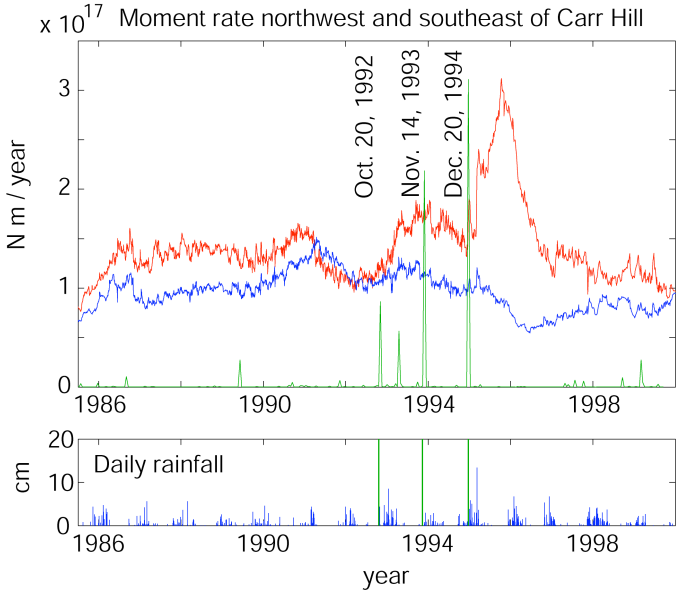

Figure 4 Moment-rate history northwest and southeast of Carr Hill. Red and blue curves in the top panel show the moment-rate from the estimated time-varying slip-rate distribution. The solution at each epoch is conditional on data only up to and including that epoch. The red curve is the rate on the northwest-most six columns of subfaults on the model fault plane, and the blue curve is that on the remaining portion of the model fault. The green curve shows the moment rate from microseismicity averaged over 15-day windows. The times of three ~M 4.5 earthquakes are indicated to the left of their corresponding spikes in moment rate. The bottom panel shows the daily rainfall for the observation period. Note the increase in rainfall in 1993 and the peak rainfall in 1995. Green lines indicate the times of the three earthquakes shown on the top panel.

The fit of this solution to the baseline time series is shown in Figure 5. Both the data and model predictions have been detrended by the observed rate of line length change up to October 20, 1992. The estimated seasonal noise has been removed from the data, and the predicted signal and random walk noise are plotted separately. The seasonal noise model successfully accounts for this noise source, as is shown by the absence of obvious annual trends in the data after removal of the seasonal estimates.

IMPLICATIONS

Two borehole tensor strainmeters, Frolich (FLT) and Eades (EDT), exhibited deviations from steady-state starting in 1993 [*Gwyther et al.*, 1996]. FLT is located northwest of Carr Hill, 2.4 km from the fault, and EDT is located 0.7 km northeast of Carr Hill near two-color

benchmark NORE (Figure 1). The observed strain changes are consistent with increased right lateral slip northwest of these stations (see discussion in *Roeloffs*, [2001]). The strain meter data have not been included in the time dependent analysis because the reliability of strainmeter measurements over periods longer than a few months is not well established, and questions remain regarding the appropriate time-dependent noise model to use for strain data. The application of the ENIF to modeling strain meter data is the subject of ongoing work.

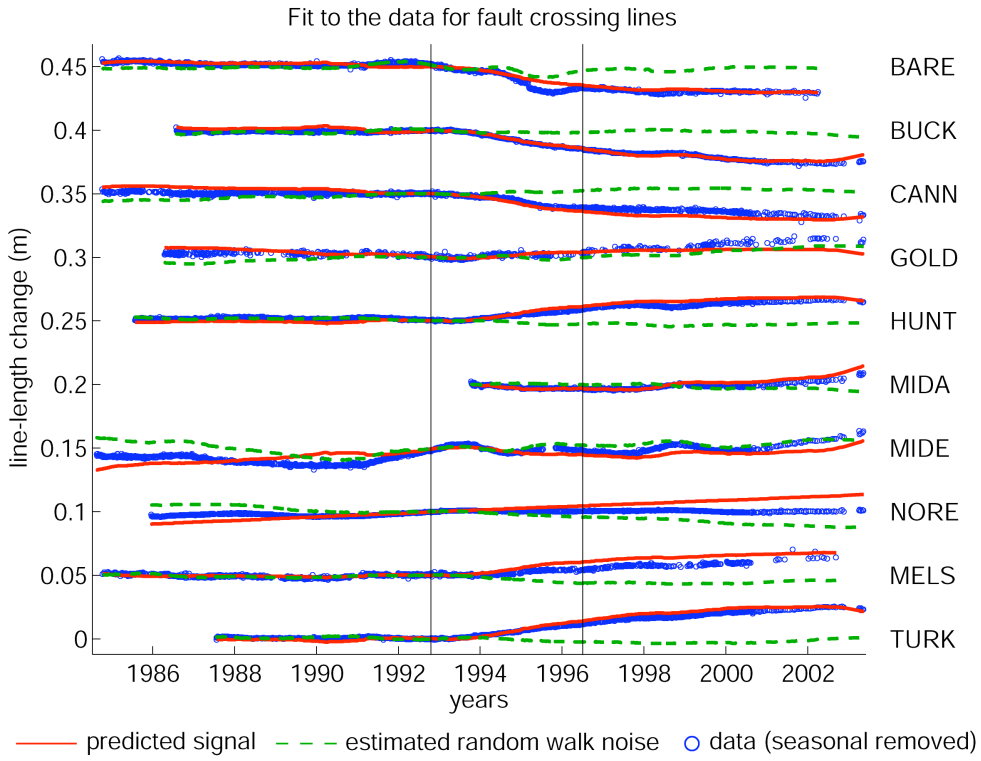

Figure 5 Observed and modeled time series from time dependent inversion for fault-crossing baselines. Blue circles are observations with the estimated seasonal displacement removed; red curves are the line lengths predicted by the estimated slip-rate history. Both are detrended using data up to October 20, 1992. The green dashed line shows the estimated random walk local motion. Black lines mark the approximate duration of the imaged slip-rate increase.

Comparison of the strain predicted from our modeled slip history to the strainmeter observations indicates that the strainmeter data require even higher slip-rate to the northwest of the strainmeter sites than we have imaged with the two color EDM data. Other studies have also concluded that the magnitude of the transient slip required by the strainmeter data is larger than that consistent with two-color EDM and creepmeter data [*Gao et al.*, 2000; *Roeloffs*, 2001]. *Langbein et al.* [1999] conducted a joint inversion of the strainmeter and two-color data and achieved a satisfactory fit to both data sets.

Deviations from the long-term trend that appeared in data from a variety of monitoring instruments in the Parkfield area during the early-to-mid 1990s are compelling evidence for an

underlying geophysical origin. However, the coincident end of a several-year drought brought increased rainfall to the area beginning in the winter of 1993 (Figure 4). The greatest rainfall between 1984 and 1998 occurred in 1995. An unusually heavy rainfall event that year is associated with an offset in the time series for station BARE [*Langbein and Johnson*, 1997]. As can be seen from Figure 5, the estimated random walk and seasonal noise account well for this local displacement. The data predicted from the fault slip solution alone does not show any sudden offset that would suggest the rainfall-induced displacement maps into the imaged slip history. The transient slip persists in the results of the time-dependent analysis, even with the BARE line omitted. Nevertheless, uncertainty remains in the effect of rainfall on the motion of the shallow monuments and, indirectly, on the fault slip rates [*Roeloffs*, 2001].

The coincidence of the ~M4.5 events and our inferred slip-rate increase lends credence to the idea that the observed two-color rate changes have a geophysical origin. The moment-rate evolution (Figure 4) inferred from the forward run of the filter implies that the slip-rate increases began following the three earthquakes. This correlation suggests that the earthquakes may have triggered transient slip.

We investigated to what extent the transient slip relieved stress increases on the fault imparted by the three moderate earthquakes. Using the detailed slip distributions obtained by *Fletcher and Spudich* [1998], we calculated the static shear stress change imposed by these events on the fault using expressions given by *Okada* [1992]. We assume that the earthquake ruptures are coplanar with the San Andreas fault, which is consistent with the earthquake relocations given their uncertainties. We calculate the stress changes at the center of each subfault assuming a shear modulus of 30 GPa. Using the Boundary Element Method, we then calculated the amount of slip on the fault surrounding the coseismic rupture areas that would be required to relieve the stress imposed by each of the three events. To avoid the stress singularities at the edge of the coseismic rupture, we omitted from the calculations stress changes at points within 500 meters of the rupture area. The cumulative slip required to relieve the stress changes from all three earthquakes is shown in Figure 6. The moment of this slip is less than 20% that of the cumulative transient slip between October 20, 1992 and July 1, 1996 northwest of Carr Hill shown in Figure 7.

The two color EDM observations used in the time-dependent inversion include any signal due to coseismic slip in the three moderate earthquakes. However, the combined moment from these events is a small fraction (<10%) of the moment of the inferred transient slip. These findings suggest that the transient event released stored strain on a portion of the fault which experiences steady-state creep at about 15 mm/yr.

Superimposed on the slip-rate distributions in Figure 3 and the cumulative transient slip distribution shown in Figure 7 are the precise relative relocations of microseismicity. These locations were obtained by *Waldhauser et al.* [2004] using a double-difference algorithm. A notable feature is the presence of sub-horizontal streaks of microseismicity, particularly on the northwestern portion of the fault plane. Two such streaks apparently bracket the hypocentral region of the 1966 M6 earthquake (Figure 7). The three ~M 4.5 earthquakes of 1992 – 1994 are indicated by blue circles in Figures 3 and 7. As discussed in *Fletcher and Spudich* [1998], these three events nucleated in the deeper of the two streaks and ruptured toward the 1966 hypocenter.

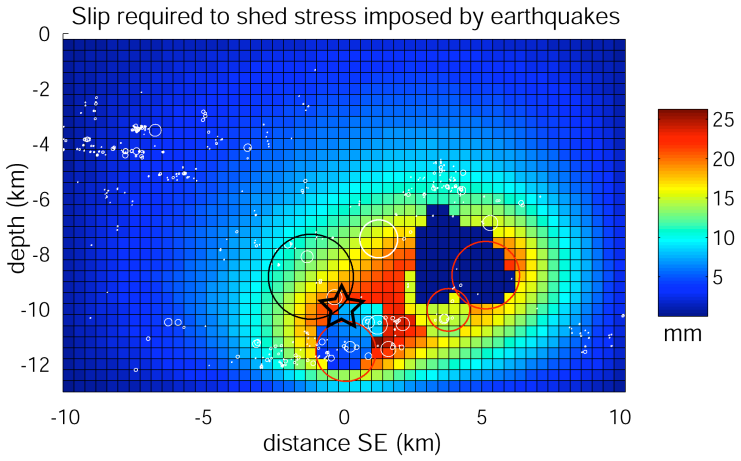

Figure 6 The cumulative slip required to relieve the shear stress increases due to the three ~M4.5 earthquakes. Superimposed is relocated microseismicity from the time period of the transient [*Waldhauser et al*., 2004]. The 1966 M6 earthquake is shown by the star, and its foreshock is shown by the black circle. The M 4.3, M 4.6, and M 4.7 events are in red. The seismicity is plotted as the equivalent rupture area of a 3 MPa stress-drop crack.

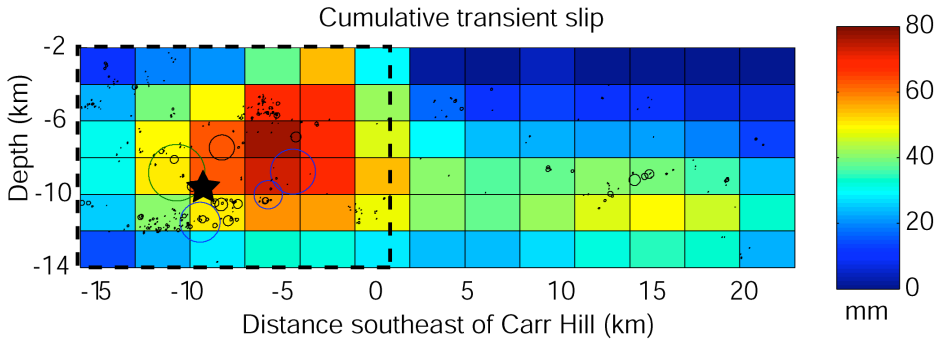

Figure 7 The estimated cumulative transient slip between October 20, 1992 and July 1, 1996 with seismicity during this time period superimposed. The black dashed box indicates the area covered in Figure 6. Background seismicity (plotted as the equivalent rupture area of a 3 MPa stress-drop crack) is shown in black and the three moderate events of the early 1990s in blue. The star marks the location of the 1966 hypocenter, and its 17-minute foreshock is shown by the green circle.

It has been suggested that streaks of microseismicity delineate areas of the fault that are locked [*Waldhauser et al.*, 2004]. A model in which the three moderate earthquakes ruptured the lower edge of a locked zone defined by the two streaks in seismicity and caused subsequent transient slip would seem to require, at least for the 1992 and 1993 events, that the transient slip propagated across the region outlined by the streaks. The transient fault slip we have imaged using the EDM data appears to initiate below 8 km depth and propagate upward over time, in keeping with the hypocentral locations of the earthquakes at 9.99 km (1992), 11.58 km (1993), and 8.86 km (1994) [*Fletcher and Spudich*, 1998]. However, given the relatively short baselines

(<10 km) of the two-color network, the resolving power for slip on this deeper part of the fault is poor, and therefore such an interpretation must be made with caution. It is apparent from Figure 3 that the peak slip-rate during the transient concentrates above the shallower of the two streaks of seismicity in the 1966 hypocentral region; the cumulative transient slip in Figure 7 is centered deeper.

In the time-dependent inversion it was possible to fit the data when transient slip was, for the length of the streaks, confined either above the upper streak or below the lower streak. However, the latter solution had essentially no transient slip northwest of Carr Hill, in disagreement with strainmeter observations. We conclude that the two-color data require slip on the portion of the fault plane above the shallower streak in seismicity.

On September 28, 2004 another M6 earthquake occurred at Parkfield [*Langbein et al.*, 2005]. This event, unlike the two previous Parkfield M6 earthquakes (and perhaps earlier ones as well), did not nucleate beneath Middle Mountain, but rather at Gold Hill, nearly 20 km to the southeast. The transient slip of the mid 1990s could have promoted another M6 earthquake at the 1966 hypocenter if it reloaded that part of the fault. However, the timing and location of the 2004 event suggest the converse. For the transient slip to have inhibited earthquake nucleation beneath Middle Mountain it would have had to reduce stress on the fault, particularly in the 1966 nucleation zone. This would be possible if the transient propagated across the area between the two streaks of seismicity. Slip between the two streaks of seismicity cannot be ruled out based on the EDM data. If transient slip did not propagate across the hypocentral region, it likely increased the shear stress at this location.

CONCLUSIONS

We have shown that temporal variations in the two-color EDM data at Parkfield are consistent with a transient increase in slip-rate on the San Andreas fault northwest of Carr Hill between late 1992 and mid 1996. This analysis accounted for the local effects of benchmark wobble and seasonal noise. The imaged slip-rate increase is consistent with that inferred from other studies of two-color EDM data, but less than that inferred from strainmeter data. The temporal relation between the imaged slip-rate increase and three moderate earthquakes in this region suggests that the seismicity triggered the slip. We infer more slip than that required to dissipate the shear stress increase due to the three earthquakes, implying that transient slip relaxed stored strain. The peak transient slip-rate concentrates above the shallower of two streaks of seismicity which bracket the nucleation zone of the 1966 M6 earthquake. We cannot resolve whether transient slip propagated across the hypocentral region of the 1966 M6 earthquake. However, the nucleation of the 2004 Parkfield M6 earthquake beneath Gold Hill rather than Middle Mountain is consistent with a reduction of stress in the hypocentral zone of the 1934 and 1966 earthquakes, perhaps due to transient slip.

REPORTS PUBLISHED

Murray, J. R. and P. Segall, Spatio-temporal evolution of a slip-rate increase on the San Andreas fault near Parkfield, CA, in review, *J. Geophys. Res*.

Murray, J. R. and P. Segall (2004), Transient slip on the San Andreas Fault: Inferences from geodetic data and the relation to moderate seismicity, *SRL, 75*, 270.

Murray, J. R. and P. Segall (2003), Analysis of data from multiple geodetic networks for a spatio-temporal fault slip history at Parkfield, CA during the 1990s, *Eos Trans. AGU,84*, Fall Meet. Suppl., Abstract G31B-0706.

Murray, J. R. and P. Segall (2002), Modeling small spatial and temporal variations in slip-rate using geodetic data, *Eos Trans. AGU, 83*, Fall Meet. Suppl., Abstract G22A-12.

Murray, J. R. and P. Segall (2002), Analysis of previously unidentified transient fault slip using geodetic data, *Eos Trans. AGU*, *83*, West. Pac. Geophys. Meet. Suppl., Abstract SE21A-06 (invited).

DATA AVAILABILITY

The two-color laser and creepmeter data may be obtained online at http://ncweb-menlo.wr.usgs.gov/research/parkfield/deform.html. Contact John Langbein (langbein@usgs.gov) for more information on data cleaning.

REFERENCES

Bakun, W.H. and A.G. Lindh (1985), The Parkfield, California earthquake prediction experiment, *Science, 229,* 619-624.

Eaton, J. P., M. E. O'Neill, and J. N. Murdock (1970), Aftershocks of the 1966 Parkfield- Cholame, California, earthquake: A detailed study, *Bull. Seismol. Soc. Am., 60,* 1151-1197.

Eberhart-Phillips, D. and A. J. Michael (1993), Three-dimensional velocity structure, seismicity, and fault structure in the Parkfield region, central California, *J. Geophys. Res., 98,* 15,737-15,758.

Fletcher, J. B. and P. Spudich (1998), Rupture characteristics of the three M ~4.7 (1992-1994) Parkfield earthquakes, *J. Geophys. Res., 103*, 835-854.

Gao, S., P. G. Silver, and A. T. Linde (2000), A comprehensive analysis of deformation data at Parkfield, CA: Detection of a long-term strain transient, *J. Geophys. Res., 105*, 2955-2967.

Gwyther, R. L., M. T. Gladwin, M. Mee, and R. H. G. Hart (1996), Anomalous shear strain at Parkfield during 1993-94, *Geophys. Res. Lett., 23*, 2425-2428.

Harris, R. and P. Segall (1987), Detection of a locked zone at depth on the Parkfield, California, segment of the San Andreas fault, *J. Geophys. Res., 92,* 7945-7962.

Hellweg, M. and J. Boatwright (1999), Mapping the rupture process of moderate earthquakes by inverting accelerograms, *J. Geophys. Res., 104*, 7319-7328.

Johnston, M. and R. Mueller (2002), Tectonomagnetic anomaly observed at Parkfield, CA from 1993 to the present - Correspondence to increased shear strain-rate during the same period, *EOS Trans. AGU*, *83*(47), Fall Meet. Suppl., Abstract G12C-05.

Langbein, J. (2004), Noise in two-color electronic distance meter measurements revisited, *J. Geophys. Res., 109*, B04406, doi:10.1029/2003JB002819.

Langbein, J. et al. (2005), Preliminary report on the 28 September 2004, M6.0 Parkfield, California, earthquake, *Seismol. Res. Lett., 76*, 1-17.

Langbein, J., R. Burford, and L. Slater (1990), Variations in fault slip and strain accumulation at Parkfield, California: Initial results using two-color geodimeter measurements, 1984-1988, *J. Geophys. Res., 95,* 2533-2552.

Langbein, J., R. L. Gwyther, R. H. G. Hart, and M. T. Gladwin (1999), Slip-rate increase at Parkfield in 1993 detected by high-precision EDM and borehole tensor strainmeters, *Geophys. Res. Lett., 26*, 2529-2532.

Langbein, J. and H. Johnson (1997), Correlated errors in geodetic time series: Implications for time-dependent deformation, *J. Geophys. Res., 102*, 591-603.

Langbein, J., M. Linker, A. McGarr, and L. Slater (1987), Precision of two-color geodimeter measurements: Results from 15 months of observations, *J. Geophys. Res., 92*, 11,644-11,656.

Langbein, J., F. Wyatt, H. Johnson, D. Hamman, and P. Zimmer (1995), Improved stability of a deeply anchored geodetic monument for deformation monitoring, *Geophys. Res. Lett., 22*, 3533-3536.

Lienkaemper, J. J. and R. D. Brown (1985), Map of faulting accompanying the 1966 Parkfield, California, earthquake, *U.S. Geol. Surv. Open File Rep.*, 85-661.

McGuire, J. and P. Segall (2003), Imaging of aseismic fault slip transients recorded by dense geodetic networks, *Geophys. J. Inter., 155*, 778-788.

Murray, J. R., P. Segall, P. Cervelli, W. Prescott, and J. Svarc (2001), Inversion of GPS data for spatially variable slip-rate on the San Andreas fault near Parkfield, CA, *Geophys. Res. Lett., 28*, 359-362.

Nadeau, R. M. and T. V. McEvilly (1999), Fault slip rates at depth from recurrence intervals of repeating microearthquakes, *Science, 285*, 718-721.

Okada, Y. (1985), Surface deformation due to shear and tensile faults in a half-space, *Bull. Seismol. Soc. Am., 75*, 1135-1154.

Okada, Y. (1992), Internal deformation due to shear and tensile faults in a half-space, *Bull. Seismol. Soc. Am., 82*, 1018-1040.

Rauch, H., F. Tung, and C. Striebel (1965), Maximum likelihood estimates of linear dynamic systems, *AIAA Journal, 3*, 1445-1450.

Roeloffs, E. (2001), Creep rate changes at Parkfield, California 1966-1999: Seasonal, precipitation induced, and tectonic, *J. Geophys. Res., 106*, 16,525-16,547.

Savage, J. C. (1990), Equivalent strike-slip earthquake cycles in half-space and lithosphere asthenosphere Earth models, *J. Geophys. Res., 95*, 4873-4879.

Segall, P. and Y. Du (1993), How similar were the 1934 and 1966 Parkfield earthquakes? *J. Geophys. Res., 98*, 4527-4538.

Segall, P. and M. Matthews (1997), Time dependent inversion of geodetic data, *J. Geophys. Res., 102*, 22,391-22,409.

Sims, J. D. (1990), Geologic map of the San Andreas fault in the Parkfield 7.5-minute quadrangle, Monterey and Fresno counties, California, *Misc. Field Studies Map MF-2115*, U.S. Geol. Surv., Menlo Park, CA.

Waldhauser, F., W. Ellsworth, D. Schaff, and A. Cole (2004), Streaks, multiplets, and holes: High-resolution spatio-temporal behavior of Parkfield seismicity, *Geophys. Res. Lett., 31*, L18608, doi:10.1029/2004GL020649.